



## Search for Neutral Higgs Boson Production in the Decay $h \rightarrow \tau_\mu \tau$ with the DØ Detector at $\sqrt{s} = 1.96$ TeV

The DØ Collaboration  
URL <http://www-d0.fnal.gov>  
(Dated: February 2, 2007)

A search for the production of neutral Higgs bosons decaying into  $\tau^+ \tau^-$  final states is presented. One of the two  $\tau$  leptons is required to decay into a muon. The data were collected by the DØ experiment at the Fermilab Tevatron Collider and correspond to an integrated luminosity of about  $1.0 \text{ fb}^{-1}$ . No excess is observed above the expected backgrounds. The results are interpreted in the Minimal Supersymmetric Standard Model. In the mass range  $90 < m_A < 200$  GeV values of  $\tan \beta$  larger than 40-60 are excluded for the no-mixing and the  $m_h^{\text{max}}$  benchmark scenarios.

*Preliminary Results for Winter 2007 Conferences*

## I. INTRODUCTION

The contribution of  $\tau^+\tau^-$  final states from the Standard Model (SM) Higgs production is too small to play any role in the SM Higgs searches in  $p\bar{p}$  collision at the Tevatron due to the large irreducible background from  $Z \rightarrow \tau^+\tau^-$  production. This is different in the Minimal Supersymmetric Standard Model (MSSM), which introduces two Higgs doublets leading to five Higgs bosons: a pair of charged Higgs boson ( $H^\pm$ ); two neutral CP-even Higgs bosons ( $h, H$ ) and a CP-odd Higgs boson ( $A$ ). At tree level, the Higgs sector of the MSSM is fully described by two parameters, which are chosen to be the mass of the CP-odd Higgs,  $m_A$ , and the ratio of the vacuum expectation values of the two Higgs doublets,  $\tan\beta$ . The Higgs production cross-section is enhanced in the region of low  $m_A$  and high  $\tan\beta$  due to the enhanced Higgs coupling to down-type fermions [1]. In the low  $m_A$ , high  $\tan\beta$  region of the parameter space, Tevatron searches can therefore probe several MSSM benchmark scenarios extending the search regions covered by LEP [2]. Inclusive searches for  $\phi(= H, h, A) \rightarrow \tau\tau$  have been performed with integrated luminosities of  $L = 350 \text{ pb}^{-1}$  by  $D\bar{O}$  [3] and  $L = 310 \text{ pb}^{-1}$  by CDF [4]. Both searches require at least one  $\tau$  lepton to decay into an electron ( $\tau_e$ ) or a muon ( $\tau_\mu$ ). In this note, only the decay  $\phi \rightarrow \tau_\mu\tau$  is considered using the full Run IIa data set with an integrated luminosity of  $L = 1.0 \text{ fb}^{-1}$ . The biggest improvement in sensitivity compared to the previous analysis comes from using a neural network to improve the separation between signal and background.

## II. DATA AND MONTE CARLO SAMPLES

The analysis is based on the data taken by the  $D\bar{O}$  experiment at the Fermilab Tevatron Collider between September 2002 and February 2006 at  $\sqrt{s} = 1.96 \text{ TeV}$ , corresponding to an integrated luminosity of  $1.0 \text{ fb}^{-1}$ . The analysis makes use of the single muon triggers, which require hits in the muon system in combination with a high momentum track in the central tracking system.

Standard Model and signal Monte Carlo events used in the analysis are generated with PYTHIA version 6.319 or 6.323 [5] and are then processed with GEANT, which provides full simulation of the detector. Monte Carlo events then undergo the same reconstruction procedure as is used for the data. All background processes, apart from QCD multi-jet and W boson production, are normalized to (N)NLO cross-sections.

## III. PRESELECTION

The preselection requires one muon to be reconstructed via a combination of hits in the muon detector and a track in the central tracking detector. The muon is required to be isolated in both the calorimeter and the tracker. The sum of the transverse energy of the calorimeter cells, in an annulus around the muon, is required to be

$$\mathcal{I}_{\text{cal}} = \sum_{\text{cells}, i} E_T^i < 2.5 \text{ GeV} \quad \text{for } 0.1 < R < 0.4, \quad (1)$$

where  $R = \sqrt{(\Delta\phi)^2 + (\Delta\eta)^2}$  is the distance in azimuth  $\phi$  and pseudorapidity  $\eta$  between the calorimeter cell and the muon direction. The isolation condition for the sum of the transverse momenta of all tracks within a cone of  $R = 0.5$  around the muon, excluding the muon track itself, is

$$\mathcal{I}_{\text{trk}} = \sum_{\text{tracks}, i} p_T^i < 2.5 \text{ GeV} \quad \text{for } 0.0 < R < 0.5. \quad (2)$$

The transverse momentum of the muon,  $p_T^\mu$  as measured from the track, is required to be greater than 15 GeV. The event is required to have no other muon that is matched to a track in the central detector with  $p_T^\mu > 10 \text{ GeV}$ .

Hadronically decaying taus are characterized by a narrow isolated jet that is associated with three or less tracks. Three types of hadronically decaying taus are distinguished:

- Type 1:** Calorimeter energy cluster, with one associated track and no electromagnetic sub-cluster. This corresponds mainly to the decay  $\tau^\pm \rightarrow \pi^\pm\nu$ .
- Type 2:** Calorimeter energy cluster, with one associated track and at least one electromagnetic sub-cluster. This corresponds mainly to the decay  $\tau^\pm \rightarrow \pi^\pm\pi^0\nu$ .
- Type 3:** Calorimeter energy cluster, with three associated tracks, with an invariant mass below 1.7 GeV. This corresponds mainly to the decays  $\tau^\pm \rightarrow \pi^\pm\pi^\pm\pi^\mp(\pi^0)\nu$ .

Tau decays into electrons are usually reconstructed as type-2 taus. These are not removed from the sample. The event is required to contain a  $\tau$  candidate at a distance  $\Delta R > 0.5$  from the muon direction. The charge of the  $\tau$  candidate, given by the sum over the charges measured from the curvature of the tracks associated with the  $\tau$  candidate, must be  $\pm 1$  and opposite to the muon charge. The transverse momentum  $p_T^\tau$  of the  $\tau$  candidate measured in the calorimeter must be greater than 15 GeV for  $\tau$ -type 1 and 2, and greater than 20 GeV for  $\tau$ -type 3. At the same time the transverse momentum of the track associated with the  $\tau$  candidate is required to be  $p_T > 15$  GeV for  $\tau$ -type 1 and  $p_T > 5$  GeV for  $\tau$ -type 2. In the case of  $\tau$ -type 3, the scalar sum of the transverse momenta of all associated tracks must be greater than 15 GeV.

#### IV. $W \rightarrow \mu\nu$ AND MULTI-JET BACKGROUND ESTIMATION

The shape of the  $W \rightarrow \mu\nu$  background distribution, where an associated jet is produced and the jet is misidentified as a tau, was simulated using PYTHIA. The normalization, however, was obtained using data. Two further selections were added to the preselection to select  $W \rightarrow \mu\nu$  events: The transverse momentum of the muon,  $p_T^\mu$ , and the missing transverse energy,  $\cancel{E}_T$ , must both be greater than 20 GeV. The  $W \rightarrow \mu\nu$  MC is then normalized to the data in the transverse mass region  $50 < M_T = \sqrt{2p_T^\mu \cancel{E}_T(1 - \cos \Delta\phi)} < 100$  GeV. The angle  $\Delta\phi$  is the angle between the direction of the muon momentum,  $p^\mu$ , and  $\cancel{E}_T$  in the  $r\phi$  plane.

A contribution to the background is expected from heavy flavour multi-jet events, where a muon from a semi-leptonic decay passes the isolation requirement and a jet is mis-identified as  $\tau$  candidate. In addition, a contribution is expected from light quark multi-jet events where the jets fake both the tau and the muon. The multi-jet background shape is taken from events with at least one muon and one  $\tau$  candidate where the muon failed the calorimeter isolation requirement. The normalization of this semi-isolated sample was obtained in a multi-jet enriched sample.

#### V. FINAL EVENT SELECTION

Since a large fraction of jets are reconstructed as tau candidates, a set of neural networks, one for each tau type, has been developed to separate the tau leptons from jets. These neural networks make use of input variables that exploit the tau signature such as longitudinal and transverse shower shapes and isolation in the calorimeter and the tracker. The neural network is trained using tau MC events as signal and multi-jet events from data as background to produce a variable that peaks near one for real taus and zero for jets. The tau candidate is required to have a neural network output greater than 0.9. In the case of type-3 taus this is tightened to 0.95 due to the larger multi-jet background.

It is also possible for muons to fake type-1 or type-2 tau candidates. These fakes are removed by ensuring that type-1 or type-2 tau candidates do not match to a reconstructed muon within a cone of radius  $\Delta R_{\mu\tau} = 0.5$ .

After selecting events with a high neural network output, there is still a considerable amount of background from W boson production in association with a jet, where the W boson decays to a muon and the jet is misidentified as a tau. To remove these events, the reconstructed W boson mass

$$M_W = \sqrt{2E^\nu E^\mu(1 - \cos \Delta\phi)} \quad (3)$$

is used, where  $E^\nu = \cancel{E}_T p^\mu / p_T^\mu$  is the estimated neutrino energy, calculated using the ratio of the muon momentum  $p^\mu$  and muon transverse momentum  $p_T^\mu$ . For real W boson decays, this variable peaks near the W boson mass, whereas for the signal and the  $Z \rightarrow \tau\tau$  background the variable peaks at zero. The distribution of  $M_W$  is shown in Figure 1. Events with  $M_W > 20$  GeV are rejected to remove most of the remaining W boson background.

The number of events observed in the data is compared to the number of expected background events in Table I for different stages of the selection. After the final selection the remaining background is dominated by the irreducible background from  $Z \rightarrow \tau\tau$ . The predicted number of events and the number of data events agree within the total systematic and statistical uncertainty.

To achieve the best separation of the signal from background, neural networks were trained for the Higgs mass points  $m_A = 90, 100, 120, 140, 160, 180, 200$  GeV using the signal MC and a weighted sum of the backgrounds. The variables used exploit the fact the signal contains a resonance at higher mass than the Z boson, and the choice of variables was optimized to get the best expected limit on Higgs production while using the same set of variables for every Higgs mass:

- The visible mass,  $M_{\text{vis}} = \sqrt{(P^\mu + P^\tau + \cancel{P}_T)^2}$ , where  $\cancel{P}_T = (\cancel{E}_T, \cancel{E}_x, \cancel{E}_y, 0)$ , and  $P^\mu$  and  $P^\tau$  are the four-vectors of the muon and tau respectively.

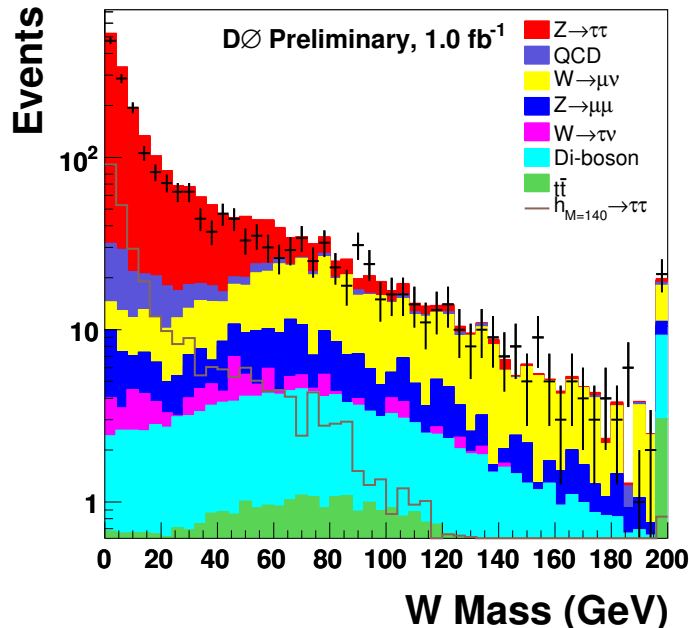


FIG. 1: Distribution of the  $W$  mass variable,  $M_W$ , with all selections other than  $M_W < 20$  GeV. The data, shown with error bars, are compared to the sum of the expected backgrounds. Also shown, as an open histogram, is the signal for a Higgs mass of 140 GeV, normalized to a cross-section of 15 pb. Overflow events are added to the last bin. Only statistical uncertainties on the data are shown.

- The transverse momentum of the muon,  $p_T^\mu$ .
- The transverse momentum of the tau,  $p_T^\tau$ , measured in the calorimeter.
- The transverse momentum of the tau, measured in the tracking detector.
- The pseudorapidity of the muon,  $\eta_\mu$ .
- The pseudorapidity of the tau,  $\eta_\tau$ .

The distribution of the visible mass  $M_{\text{vis}}$  is shown in Figure 2. The distribution of the optimised neural networks for Higgs masses of 160 GeV and 180 GeV are shown in Figures 3 and 4 for the three tau types separately and for the total data set. There is good agreement between the background expectation and the data.

## VI. RESULTS

Since the data are consistent with a background only observation, limits on the cross-section for Higgs boson production times the branching fraction into tau leptons are derived at 95% Confidence Level (CL). To maximise the sensitivity, the output from the neural networks, shown in Figures 3 and 4 for two mass points, are used in the limit calculation. The distributions for the three tau types are used separately to exploit the different signal to background ratios. The cross-section limits are calculated with the  $\text{CL}_S$  method [6].

There are various sources of systematic uncertainties that affect signal and background. The most important are the uncertainty on the integrated luminosity (6.1%), the trigger efficiency (3%), the tau energy scale (1 – 11%), the uncertainty in the signal acceptance due to choice of parton distribution function (3.9–4.6%), the uncertainty of the tau track matching efficiency (4%), the uncertainty on the tau reconstruction efficiency (3%), the theoretical uncertainty on the  $Z$  cross-section (5%) and the uncertainty on the modeling of the multi-jet background (3%). All systematic uncertainties are included in the calculation of the expected and observed limits, assuming 100% correlation between

Process	Selection			
	Pre-selection	NN $_{\tau} > 0.9$ (0.95 type 3)	$\Delta R_{\mu\tau} > 0.5$	$M_W < 20$ GeV
$Z \rightarrow \tau\tau$	2301	1612	1607	$1163 \pm 127$
$Z \rightarrow \mu\mu$	934	197	114	$18 \pm 3$
$W \rightarrow \mu\nu$	8688	349	347	$26 \pm 5$
$W \rightarrow \tau\nu$	717	25	25	$7 \pm 1$
$WW \rightarrow \ell\nu\ell\nu$	105	93	93	$8.4 \pm 0.8$
WZ	28	5.7	5.7	$0.8 \pm 0.1$
ZZ	5	1.6	1.6	$0.5 \pm 0.2$
$t\bar{t}$	191	36	36	$3.3 \pm 0.3$
QCD	4326	109	108	$60 \pm 30$
Predicted	17295	2429	2337	$1287 \pm 130$
Data	17425	2146	2075	1144
$\epsilon(m_{\phi} = 140$ GeV)	2.9%	2.2%	2.2%	1.4%

TABLE I: Number of data events and expected number of background events after applying the preselection, the selection on the  $\tau$  neural net output,  $NN_{\tau} > 0.9$ , the selection rejecting events where muon and  $\tau$  overlap,  $\Delta R_{\mu\tau} > 0.5$ , and the selection requiring  $M_W < 20$  GeV ( $\ell = e, \mu, \tau$ ). Also shown is the efficiency  $\epsilon$  for the signal process  $\phi \rightarrow \tau^+\tau^-$  with a Higgs mass of 140 GeV. The uncertainties represent the quadratic sum of the systematic uncertainties and the statistical uncertainties of the Monte Carlo.

signal and background where appropriate. The expected and observed limits are shown in Figure 5 as a function of the hypothetical Higgs mass.

In the MSSM, the masses and couplings of the Higgs bosons depend on  $\tan\beta$  and  $m_A$  at tree level. Radiative corrections introduce additional dependencies on SUSY parameters. In a constrained model, where unification of the SU(2) and U(1) gaugino masses is assumed, the most relevant parameters are

- the mixing parameter  $X_t$ ;
- The mass parameter  $\mu$ ;
- the gaugino mass term  $M_2$ ;
- the gluino mass  $m_{\tilde{g}}$ ;
- the common scalar mass  $M_{\text{SUSY}}$ .

In this analysis, the  $m_h^{\text{max}}$  and no-mixing scenarios are studied. The scenarios have the following parameters:

- $m_h^{\text{max}}$  scenario:
  - $X_t = 2$  TeV;
  - $\mu = \pm 0.2$  TeV;
  - $M_2 = 0.2$  TeV;
  - $m_{\tilde{g}} = 0.8$  TeV;
  - $M_{\text{SUSY}} = 1$  TeV.
- No-mixing scenario:
  - $X_t = 0$  TeV;
  - $\mu = \pm 0.2$  TeV;
  - $M_2 = 0.2$  TeV;
  - $m_{\tilde{g}} = 1.6$  TeV;
  - $M_{\text{SUSY}} = 2$  TeV.

The cross-section and branching ratios of the Higgs bosons within each scenario have been calculated with FeynHiggs 2.5.1 [7] using the U-matrix approximation [8].

The corresponding excluded regions in the  $\tan\beta - m_A$  plane are shown in Figure 6, for the case when  $\mu < 0$ , and in Figure 7 for the case then  $\mu > 0$ . The cross-section at each  $\tan\beta - m_A$  point was calculated by adding the  $gg \rightarrow \phi$  and  $b\bar{b} \rightarrow \phi$  cross-sections for a given  $m_A$ . The cross-section for  $h$  or  $H$  production was added if  $|m_{h,H} - m_A| < 15$  GeV.

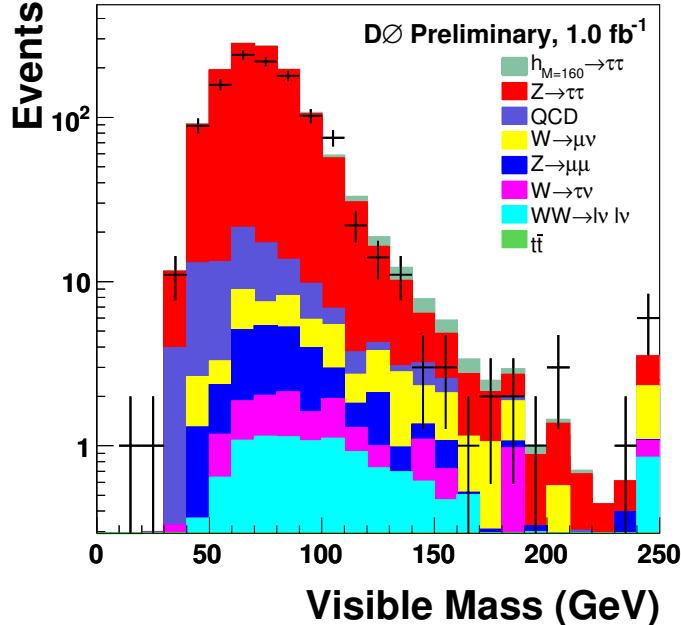


FIG. 2: Distribution of the visible mass  $M_{\text{vis}}$  with all selections applied. The data, shown with error bars, are compared to the sum of the expected backgrounds. Overflow events are added to the last bin. Also shown, in light green, is the signal for a Higgs mass of 160 GeV, normalized to the cross-section excluded by this analysis. Only statistical uncertainties on the data are shown. The systematic uncertainty on the background normalisation is 10%.

## VII. CONCLUSION

A search for the production of neutral Higgs boson decaying into tau leptons in  $p\bar{p}$  collisions at  $\sqrt{s} = 1.96$  TeV was performed using a data set corresponding to an integrated luminosity of  $1.0 \text{ fb}^{-1}$ . One of the tau leptons is identified through its decay into a muon. In the mass region  $90 < m_A < 200$  GeV,  $\tan\beta$  values larger than 40-60 are excluded for the no-mixing and the  $m_h^{\text{max}}$  benchmark scenarios. These results are the most constraining limits from the Higgs to  $\tau^+\tau^-$  decay channel to date.

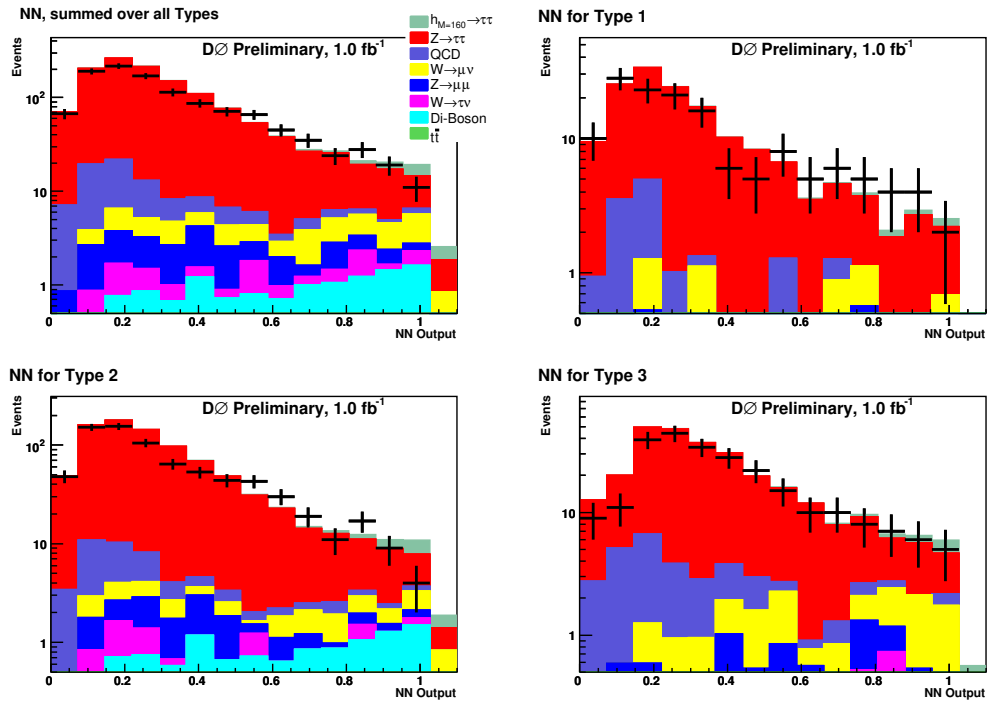


FIG. 3: Neural network output distribution for a Higgs mass of 160 GeV for the sum of the expected backgrounds and the signal, shown in light green. The signal is normalized to the cross-section excluded by the analysis. a) sum over all tau types, b) type 1, c) type 2 and d) type 3. Only statistical uncertainties on the data are shown. The systematic uncertainty on the background normalisation is 10%.

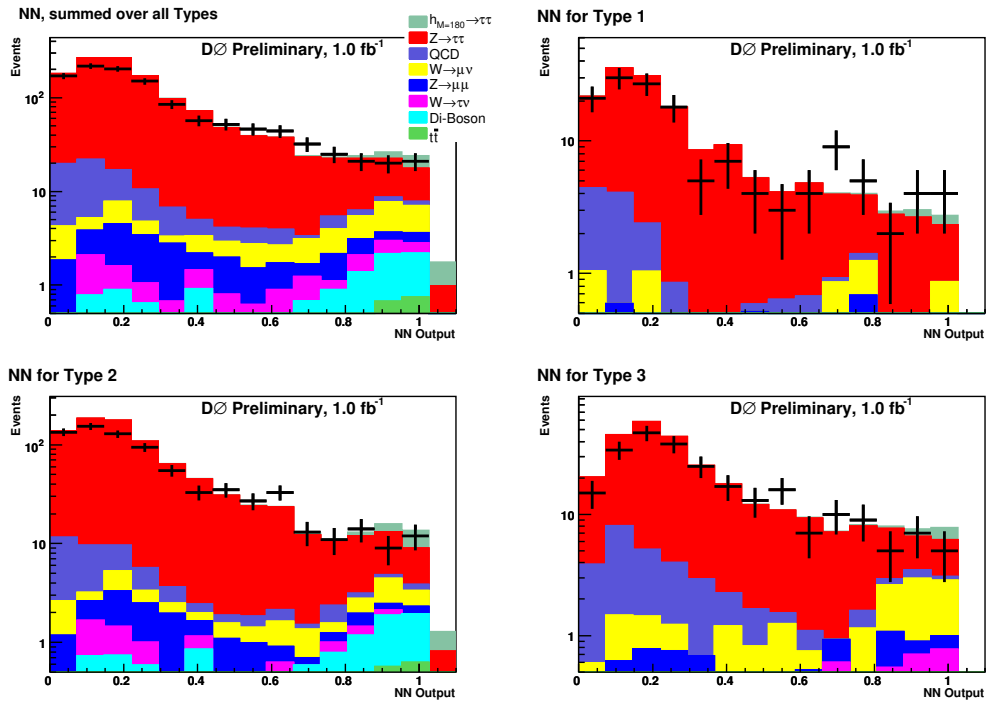


FIG. 4: Neural network output distribution for a Higgs mass of 180 GeV for the sum of the expected backgrounds and the signal, shown in light green. The signal is normalized to the cross-section excluded by the analysis. a) sum over all tau types, b) type 1, c) type 2 and d) type 3. Only statistical uncertainties on the data are shown. The systematic uncertainty on the background normalisation is 10%.

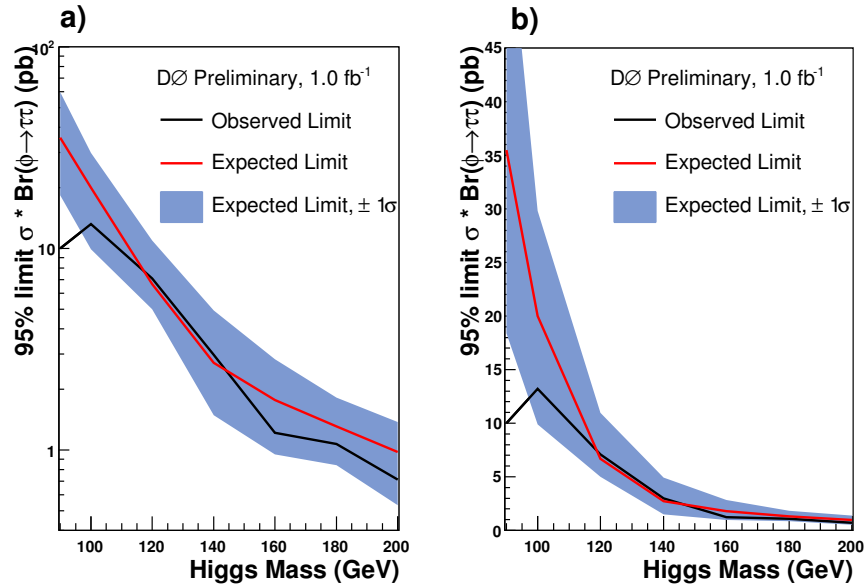


FIG. 5: Observed and expected 95% Confidence Level upper limit on the cross-section times branching ratio, using the neural network shown on a) a log scale and b) a linear scale. The band represents the  $\pm 1\sigma$  uncertainty on the expected limit.

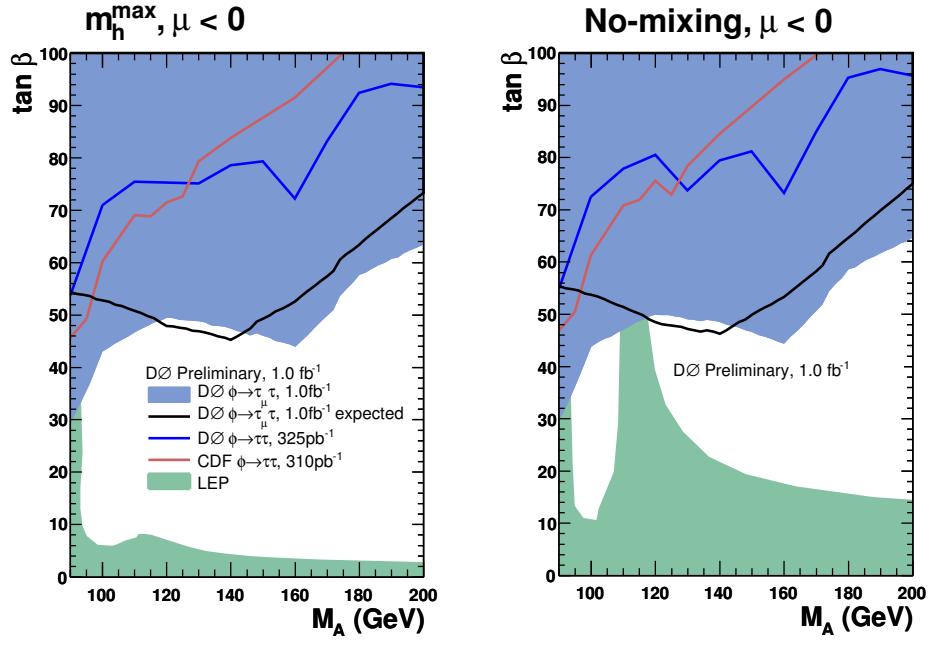


FIG. 6: Excluded region in the  $\tan\beta - m_A$  plane for  $\mu < 0$  in a) the  $m_h^{\max}$  scenario and b) the no-mixing scenario. Also shown is the LEP limit [2], the CDF results for  $\phi \rightarrow \tau\tau$  [4] and the previous  $D\phi \rightarrow \tau\tau$  result [3].

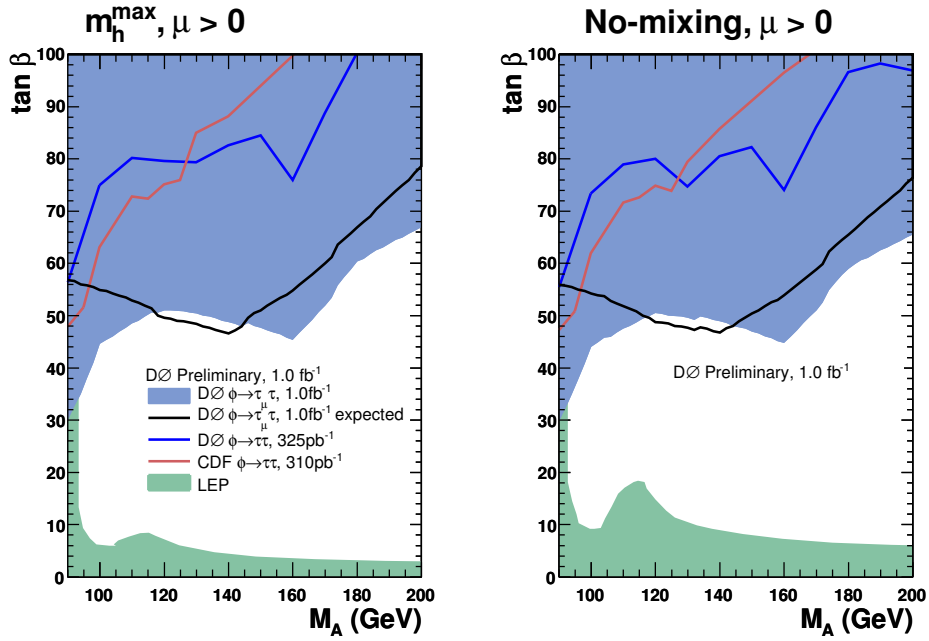


FIG. 7: Excluded region in the  $\tan\beta - m_A$  plane for  $\mu > 0$  in a) the  $m_h^{\max}$  scenario and b) the no-mixing scenario. Also shown is the LEP limit [2], the CDF results for  $\phi \rightarrow \tau\tau$  [4] and the previous  $D\phi \rightarrow \tau\tau$  result [3].

### Acknowledgments

We thank the staffs at Fermilab and collaborating institutions, and acknowledge support from the DOE and NSF (USA); CEA and CNRS/IN2P3 (France); FASI, Rosatom and RFBR (Russia); CAPES, CNPq, FAPERJ, FAPESP and FUNDUNESP (Brazil); DAE and DST (India); Colciencias (Colombia); CONACyT (Mexico); KRF and KOSEF (Korea); CONICET and UBACyT (Argentina); FOM (The Netherlands); PPARC (United Kingdom); MSMT (Czech Republic); CRC Program, CFI, NSERC and WestGrid Project (Canada); BMBF and DFG (Germany); SFI (Ireland); The Swedish Research Council (Sweden); Research Corporation; Alexander von Humboldt Foundation; and the Marie Curie Program.

- 
- [1] M. Carena, S. Heinemeyer, C.E.M Wagner and G. Weiglein, *Eur. Phys. J. C* **45** (2006) 797.
  - [2] The ALEPH, DELPHI, L3 and OPAL Collaborations, LHWG-Note 2005-01.
  - [3] V.M. Abazov *et al.*, *Phys. Rev. Lett.* **97** (2006) 121802.
  - [4] A. Abulencia *et al.*, *Phys. Rev. Lett.* **96** (2006) 011802.
  - [5] T. Sjöstrand *et al.*, *Comput. Phys. Commun.* **135** (2001) 238.
  - [6] R. Barate *et al.*, *Phys. Lett. B* **565** (2003) 61; T. Junk, *Nucl. Instrum. Meth. A* **434** (1999) 435.
  - [7] S. Heinemeyer, W. Hollik, G. Weiglein, *Comput. Phys. Commun.* **124** (2000) 76.
  - [8] S. Heinemeyer, private communications.